The 2025 World Congress on
Advances in Structural Engineering and Mechanics (ASEM25)
BEXCO, Busan, Korea, August 11-14, 2025

Analysis of Chamber Grouting Mechanism ahead of TBM Face Using Numerical Analysis

Pill-Bae Hwang[1], Terry Moon[2], and Seok-Won Lee*[3]

[1)] PhD Student, Dept. of Civil and Environmental Engr, Konkuk University, Seoul, R. of Korea
[2)] Master Student, Dept. of Civil and Environmental Engr, Konkuk University, Seoul, R. of Korea
[3)] Professor, Dept. of Civil and Environmental Engr, Konkuk University, Seoul, R. of Korea

ABSTRACT

The cutters of TBM get worn due to continuous excavation, mixed ground conditions and other factors. This wear causes the decrease in TBM excavation efficiency and the excessive increase in torque. Therefore, inspecting and replacing the cutters during tunnel excavation is of critical importance. Since cutter inspection and replacement require the release of face pressure, stabilizing the tunnel face must be prioritized. The process of inspecting and replacing the excavation tools attached to the TBM cutterhead is referred to as Cutterhead Intervention (CHI). When performing CHI in tunnels with great depth and high water pressure, such as under the sea or in the ocean, the work must be performed in response to high external pressure and a large water inflow into the chamber. In such cases, it is necessary to perform chamber grouting in front of the tunnel face. However, the chamber grouting mechanism for proper water inflow reduction and hydraulic pressure reduction have not yet been elucidated. In this study, the phenomena occurring when grout is penetrated into the front of the tunnel face to perform CHI were investigated using numerical analysis. The Herschel-Bulkely model and the VOF (Volume of Fluid) model provided by the FLUENT code are applied to simulate the grout flow in the voids of soil particles filled with water. Finally, the effects of reducing water inflow according to the characteristics of the grout solution, the change in the injection amount and the injection pressure are investigated. The particle behavior which changes as the grout solution infiltration is also analyzed.

1. INTRODUCTION

Due to the saturation of aboveground spaces driven by the advancement of modern

---

[1] Phd Student
[2] Master Student
[*3] Professor (corresponding Author)

society, the utilization of underground spaces is increasing. Among underground facilities, tunnels offer greater environmental benefits and reduce social costs compared to other structures, resulting in growing demand for their construction. When constructing tunnels at significant depths with high external pressures such as underwater or seabed conditions, shield TBMs are typically applied. TBM mounts various excavation tools, such as disc cutters and cutter bits, onto the cutterhead. The cutterhead rotates to excavate the ground. Because the excavation tools are fixed to the cutterhead, slipping can occur between the cutters and the rock, generating reactive forces that lead to tool wear. This wear reduces tunneling efficiency and results in excessive torque during shield TBM operation. Therefore, inspecting and replacing cutters during tunnel excavation is critically important. Currently, workers must enter the high pressure chamber through a man lock to inspect and replace the cutters, enduring the pressurized environment. Depending on ground conditions, a significant inflow of water into the chamber can render the work impossible, thereby extending the construction period. To address these challenges, previous studies (Hwang et al., 2024) have proposed a chamber grouting mechanism applied in front of the TBM face from the TBM chamber without requiring additional equipment to stabilize the TBM face. This study aims to develop a numerical model for the newly proposed chamber grouting method. To this end, this study combines the VOF (Volume of Fluid) model and the DEM (Distinct Element Method) model provided by the FLUENT code to analyze the fluid flow of the grout solution and the behavior of soil particles, thereby simulating grout flow within water-filled soil pores. Through this, the penetration distance of the grout solution according to the change in grout injection pressure and ground conditions were investigated and the effect of reducing the amount of inflow water flowing into the TBM face were studied.

2. Numerical Modeling of Grouting Mechanism Ahead of the TBM Face

2.1 Ansys Fluent Program

In saturated sandy soil, the fluid behavior of the grout solution during the grouting process is determined by interactions with soil particles and the surrounding fluid. The movement of particles is governed by Newton's laws of motion and is modeled using the DEM (Distinct Element Method), which detects particle collisions and calculates contact forces. To simulate particle interactions in sandy soils characterized by low cohesion and wide particle size distribution, the Hertz-Mindlin model (no-slip) was applied. Meanwhile, cement grout behaves as a non-Newtonian fluid, specifically exhibiting the characteristics of a Bingham fluid. Bingham fluids are typically described by yield stress and viscosity, and the FLUENT code supports the VOF (Volume of Fluid) model for analyzing such fluids. The VOF model is an ideal flow model capable of accurately simulating interfaces between slurry and water, including slug flow, stratified flow, and free-surface flow. Based on the VOF model, ANSYS FLUENT serves as a suitable numerical analysis program for simulating grout flow. Ultimately, in this study, the VOF-DEM analysis process was implemented using the computational fluid dynamics software ANSYS FLUENT and the DEM software EDEM (Engineering Discrete Element Method), which simulates the microscopic behavior of granular materials such as sand or soil. The flowchart of this process is shown in **Fig. 1**.

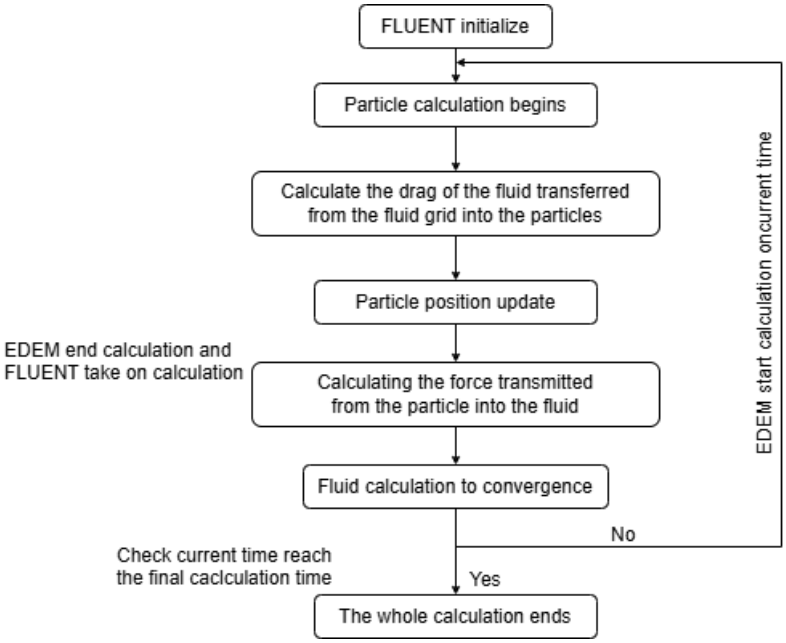

Fig. 1 Flowchart of VOF-DEM Model Execution (Li et al., 2022)

2.2 Numerical Modeling Process

ANSYS FLUENT is software for analyzing fluid behavior. As shown in **Fig. 2**. it generates a virtual mesh space, and by setting fluid properties such as viscosity and pressure, it enables observation of the resulting fluid behavior.

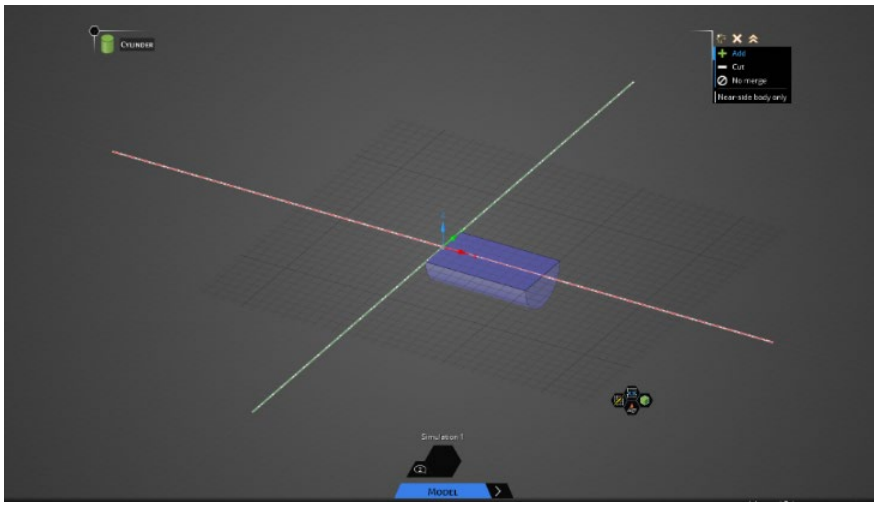

Fig. 2 ANSYS FLUENT Mesh Setup

The main purpose of this study is to numerically verify and extend the results of the previous study (Hwang et al., 2024) performed experimentally. Therefore, the numerical analysis model also simulates the experimental equipment of the previous study (Hwang et al., 2024). The virtual space (mesh) was designed to simulate the model ground and TBM as shown in **Fig. 3**. The soil chamber where the TBM excavation is performed was 60 cm long, 40 cm wide, and 85 cm high, and was constructed so that the TBM could be located in the center. The model shield TBM, which injects grout in front of the tunnel face, was constructed with a diameter of 20 cm and a length of 10 cm. The soil particles constituting the model ground were assumed to be round sandy soil, and the particle diameter was set to 2.86 mm.

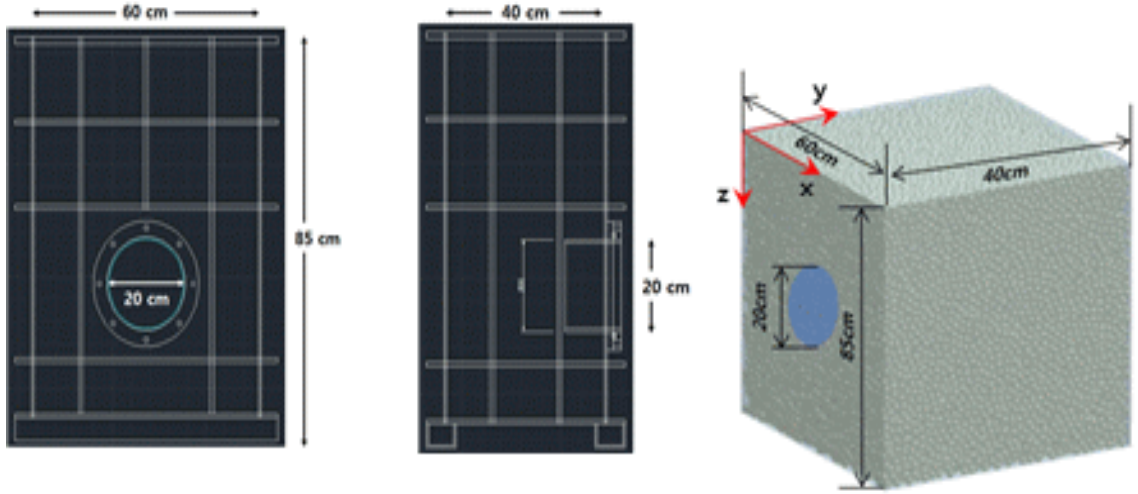

Fig. 3 Model Ground Implemented Using Numerical Analysis Software

Sandy soil generally forms a conical shape during deposition because particles align in specific directions, creating an inherent angle of repose. This characteristic can serve as a calibration criterion for contact parameters in particle-based simulations using the DEM (Discrete Element Method) (Ghazavi et al., 2008). Currently, modeling the sand layer requires representing a large number of sand particles. As the number of particles increases, the program's computational speed decreases, and the likelihood of calculation errors increases. Accordingly, in this study, the number of soil particles was limited by increasing the particle diameter of sandy soil to less than 10 times to increase the simulation speed. The impact of this modification on the mechanical behavior of actual sandy ground was investigated through an angle of repose model test, as shown in **Fig. 4**. Through this process, three ground conditions with porosities of 0.3, 0.35, and 0.4 were established. The relative densities of the soils composed of each porosity are 76.6, 59.1, and 38.4, respectively. Subsequently, an overburden load was applied to the top of the model ground, the planned injection pressure was exerted, and grout solution was injected ahead of the TBM face. After injection was completed, the volume of water

inflow flowing into the TBM face and the grout penetration distance were measured.

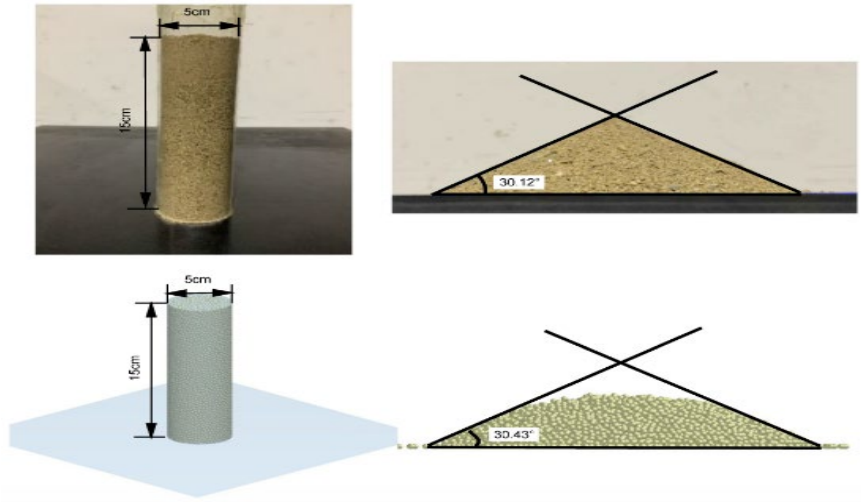

Fig. 4 Standard and Simulated Particles: Repose Angle Test

3. Water inflow according to grout injection pressure and ground conditions

The volume of water inflow into the tunnel face was measured according to variations in grout injection pressure and ground conditions. To quantitatively compare the reduction in water inflow due to grout injection, it is first necessary to estimate the inflow quantity into the tunnel face in the ground without grouting. Accordingly, numerical analyses were conducted under three ground conditions with porosities (n) of 0.3, 0.35, and 0.4, considering only the application of overburden pressure without grout injection. The results, presented in **Fig. 5**, show that the water inflow increases consistently with higher overburden pressure and looser ground conditions (i.e., higher porosity).

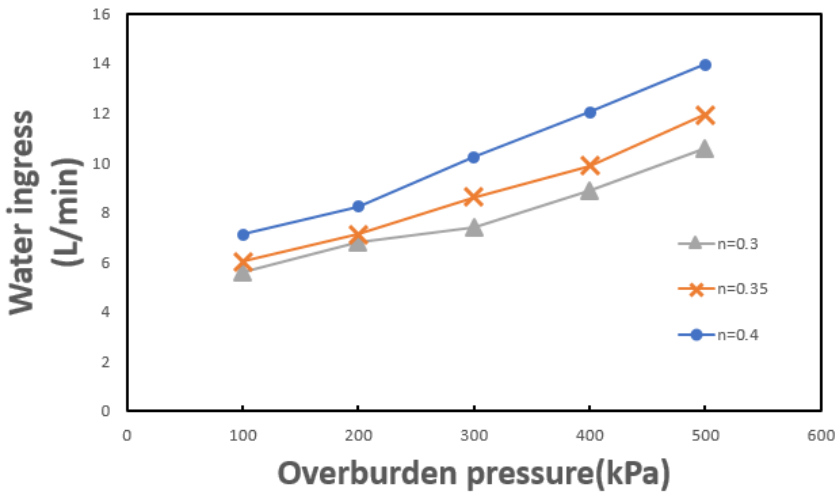

Fig. 5 Results of Water Inflow in the Ground without grouting

The volume of water inflow into the tunnel, measured through numerical analysis in response to changes in injection pressure, is presented in **Fig. 6**. The overburden pressure was fixed at 500 kPa, the same as in the TBM model test of a previous study (Hwang et al., 2024). The inflow reduction rate is defined as the percentage decrease in inflow compared to the baseline condition without grout injection (see **Fig. 5**). For the case with a porosity of n = 0.3, the inflow reduction rate did not show a significant change under low grout injection pressures, but began to gradually increase beyond a certain injection pressure. In contrast, for n = 0.4 and n = 0.5, a notable and sharp increase in the inflow reduction rate was observed after a specific injection pressure threshold. This behavior can be explained with reference to **Fig. 7**, which illustrates the diffusion pattern of grout during injection. In the case of n = 0.3, as shown in **Fig. 7(c)**, grout penetration was limited to the central part of the TBM chamber, resulting in a gradual rather than abrupt reduction in inflow. On the other hand, in the cases of n = 0.4 and n = 0.5, as shown in **Fig. 7(d)** and **Fig. 7(e)**, respectively, the grout penetration behavior transitioned from a centralized penetration confined within the TBM chamber diameter to a diffusive penetration extending beyond the chamber boundary as the injection pressure increased. Notably, the injection pressure at which the inflow reduction rate begins to sharply increase coincides with the point where this behavioral transition occurs. Therefore, in relatively loose ground conditions, a sufficient increase in injection pressure is required to induce diffusive penetration behavior, which significantly enhances the water inflow reduction effect. However, in dense sandy ground with n = 0.3, even a substantial increase in injection pressure results only in centralized penetration within the TBM chamber diameter, and this limitation should be acknowledged.

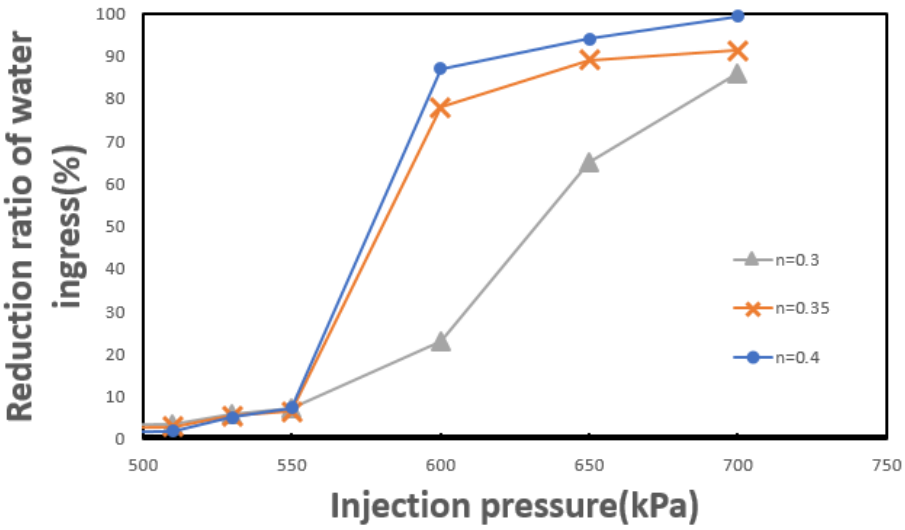

Fig. 6 Inflow Volume Reduction Rate According to Changes in Injection Pressure

4. Grout Penetration Change by Injection Pressure and Ground Conditions

The grout penetration distance was numerically estimated under varying ground conditions and grout injection pressures. These results were then compared with those obtained from existing analytical formulations to evaluate both the validity and scalability of the numerical analysis conducted in this study, as well as the applicability of the conventional theoretical models.

4.1 Numerical Analysis of Grout Penetration Distance

In the numerical analysis, the overburden pressure was set to 500 kPa, identical to that used in the experimental TBM model test (Hwang et al, 2024). Grout injection pressures were varied across six levels(510, 530, 550, 600, 650, and 700 kPa) while the porosity (n) of the ground was considered at five levels(0.1, 0.2, 0.3, 0.35, and 0.4). Accordingly, a total of 30 simulation cases were analyzed, combining different ground conditions and injection pressures.

In each simulation, the grout was introduced into the ground model at the specified injection pressure, and the resulting displacement vectors were recorded to visualize the grout penetration. Once the displacement stabilized(indicating the completion of grout flow), the final penetration pattern was plotted, as shown in **Fig. 7**.

Fig. 7(a) presents the results for n = 0.1, illustrating the injection range of grout under the six pressure conditions. In this context, the y-axis represents the TBM tunnel face, and grout penetrates in the x-direction from the center of the TBM chamber. Due to the highly dense nature of the ground at n = 0.1, grout infiltration was negligible under all tested injection pressures. The grout spread pattern remained flat, showing little to no penetration. **Fig. 7(b)** shows the results for n = 0.2. Although some limited penetration of grout was observed, uniform infiltration was not achieved. At injection pressures of 510 to 600 kPa, the penetration pattern was similar to that at n = 0.1(flat and negligible). Only at 650 and 700 kPa did a small amount of grout begin to infiltrate the ground. In **Fig. 7(c)**, corresponding to n = 0.3, significant grout penetration begins to appear at pressures above 600 kPa. However, the infiltration remains concentrated around the chamber center, expanding in a bell-shaped pattern without wide diffusion in the vertical (y) direction. **Figs. 7(d)** and **7(e)** show the results for loose ground conditions with porosities of n = 0.35 and 0.4, respectively. In these cases, grout infiltrates not only in front of the TBM face but also diffuses more broadly compared to the denser ground conditions. Specifically, up to 530 kPa, the penetration remains minimal, as in the previous cases. At 550 kPa, penetration initiates in a bell-shaped, centrally focused pattern. However, at 600 kPa and higher, infiltration in the vertical direction (y-axis) significantly increases, resulting in a pot-shaped spread pattern, referred to here as diffusive penetration behavior.

These findings are consistent with the previously discussed water inflow reduction results. In very dense sandy ground (n = 0.1~0.2), diffusive penetration does not occur, and the grout spread remains limited. In contrast, looser soils with higher porosity allow for easier infiltration due to the wider spacing between particles. Furthermore, at

sufficiently high injection pressures, it can be inferred that hydraulic fracturing and forced displacement of particles occur, facilitating more extensive grout propagation.

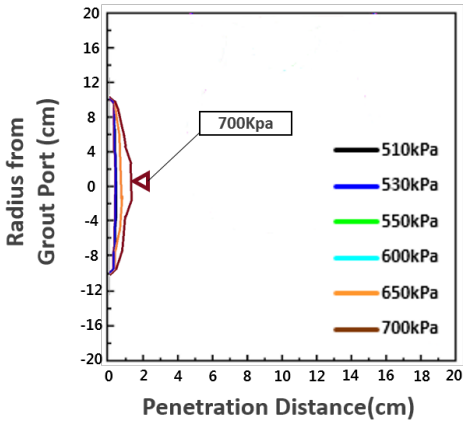

(a) n=0.1

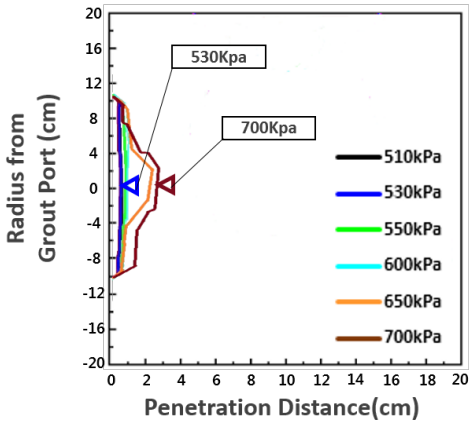

(b) n=0.2

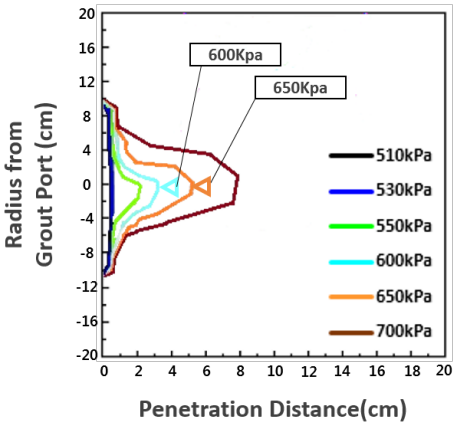

(c) n=0.3

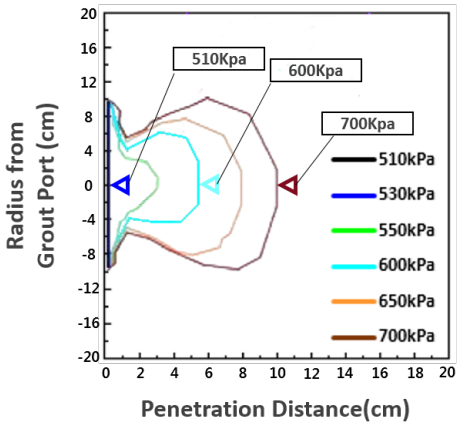

(d) n=0.35

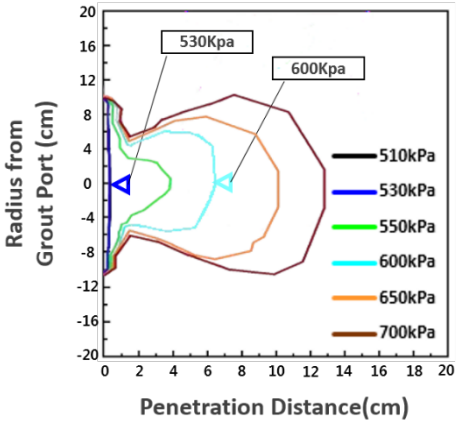

(e) n=0.4

Fig. 7 Grout Injection Range According to Porosity

4.2 Theoretical Analysis of Grout Penetration Distance

The fluid analysis model for cement-based grout utilizes the Bingham Fluid Plastic Model, a type of non-Newtonian fluid model. A Bingham fluid behaves like a solid under low shear stress and flows like a fluid when the shear stress exceeds a specific yield stress, known as the yield stress of the Bingham fluid. Raffle and Greenwood (1961) proposed the pressure gradient (i) required to overcome this yield stress, expressed in Eq. (1). Here, τ_s represents the yield stress of the Bingham fluid, and d denotes the effective radius of the average pore.

$$\mathrm{i} = \frac{4\tau_s}{d} \tag{1}$$

A Bingham fluid requires an additional pressure gradient to maintain continuous flow. To determine the effective radius (d) of the average pore, Bruce et al. (1994) proposed **Eq. (2)** derived from the Kozeny-Carman equation. Here, δ_w represents the density of water, g is the gravitational acceleration, k is the soil permeability coefficient (m/s), μ is the viscosity of the grout (cp), and n denotes the porosity.

$$\mathrm{d} = 2\sqrt{\frac{8\mu k}{\delta_w g n}} \tag{2}$$

The effective radius (d) of the average pore, calculated through the above process, is substituted into **Eq. (3)** to determine the penetration limit distance. Here, H represents the grout pressure head, and r denotes the grout injection radius.

$$\mathrm{R}_L = \frac{\delta_w g H d}{4\tau_s} + r \tag{3}$$

Grouting can be understood as the process by which grout material penetrates the soil. In this process, the permeability coefficient (k) serves as a key parameter in models describing infiltration and diffusion. Generally, this value is obtained through experiments, however when experiments are not feasible, an empirical estimation is required. In this regard, Shepherd (1989) proposed a modified Hazen equation, presented in **Eq. (4)**, which adjusts the traditional Hazen formula to better reflect actual field conditions and construction outcomes. Using this modified equation, the permeability coefficient can be estimated based on the median grain size (D_{50}).

$$\mathrm{k}(cm/sec) = 0.0710 \times \{D_{50}(mm)\}^{1.60} \tag{4}$$

The flow behavior of grout is typically analyzed using the Bingham fluid model, which considers yield stress and plastic viscosity as the primary parameters. These properties reflect the characteristics of the grout at the beginning of the injection process. While

these parameters are usually measured directly through experiments, they can also be estimated from literature when experimental data are unavailable. For example, Lee (2021) measured viscosity according to ASTM D2196 after mixing ordinary Portland cement, water, and bentonite in fixed proportions; the results are presented in **Fig. 8**. Additionally, Benyounes (2019) analyzed changes in yield stress according to bentonite content at a water-to-cement ratio of 1.0, with the results shown in **Fig. 9**.

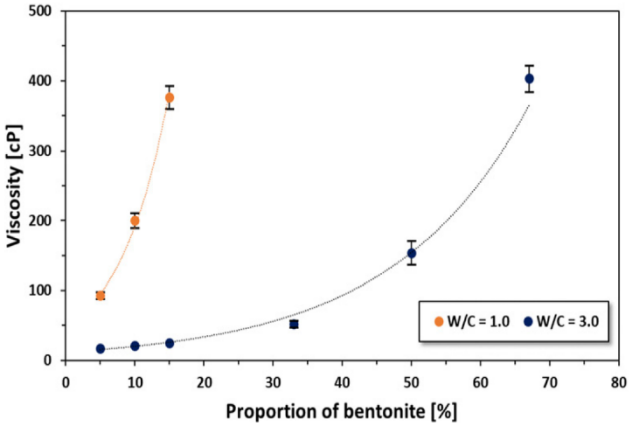

Fig. 8 Viscosity with proportion of bentonite and W/C (Lee, 2021)

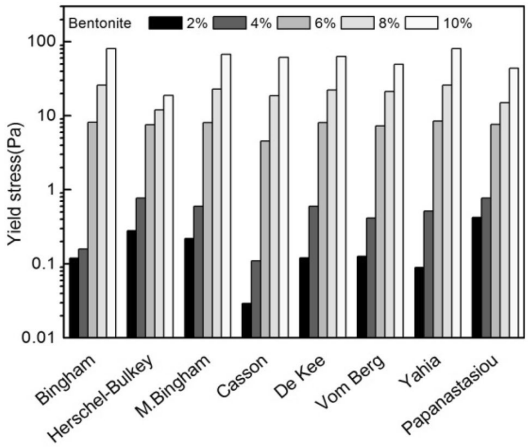

Fig. 9 Yield Stress of Bingham Fluid (Beyones, 2019)

In conclusion, the previously proposed theoretical model for grout penetration and diffusion was applied to calculate the theoretical penetration limit under three ground conditions, assuming sand with a grain size of 2.86 mm and porosities of 0.3, 0.35, and 0.4, matching those used in the numerical analysis. By comparing these theoretical estimates with the numerical results discussed earlier, the validity of both the numerical approach and the theoretical model used in this study can be evaluated.

The grout penetration distance based on the theoretical model was estimated through the following procedure. First, the grout used in the numerical analysis was assumed to be a cement-based grout with a water-to-cement ratio (W/C) of 1.0 and 8% bentonite content by weight of water. The yield stress and plastic viscosity of this grout were determined to be 27 Pa and 170 cP, respectively, based on experimental data shown **in Fig. 8** and **Fig. 9**.

For the calculation of the permeability coefficient (k), the median particle size (D_{50}) was derived using regression data from Cubrinovski and Ishihara (1999, 2002), who compiled maximum and minimum void ratios and D_{50} values for various sandy soils. These values were applied to **Eq. (4)** to calculate k for each porosity condition (0.3, 0.35, and 0.4). Using the obtained permeability values and the grout's rheological properties, the effective radius of the average pore (d) was calculated using **Eq. (2)**, and subsequently, the theoretical grout penetration distance was estimated using **Eq. (3)**. All

calculated results are summarized in **Table 1**. It is important to note that the theoretical penetration distances calculated using the model are based solely on permeation grouting, under the assumption that no hydraulic fracturing occurs. Therefore, under identical conditions, the diffusion distance predicted for permeation-only grouting is expected to be greater than that associated with fracture-induced diffusion.

Table 1 Theoretical Penetration Limit Distances According to Porosity

Porosity	Permeability coefficient (cm/s)	Effective radius of average pore	Penetration limit distance
0.30	7.627×10^{-4}(m)	1.198×10^{-4}(m)	$R_L = 0.0435P_o + r_o(cm)$
0.35	1.432×10^{-3}(m)	1.524×10^{-4}(m)	$R_L = 0.0701P_o + r_o(cm)$
0.40	2.565×10^{-3}(m)	1.868×10^{-4}(m)	$R_L = 0.0887P_o + r_o(cm)$

4.3 Numerical and Analytical Comparison of Grout Penetration Distances

The comparison between grout penetration distances calculated using the theoretical equation and those obtained from numerical analysis is presented in **Fig. 10**. As shown in **Fig. 10(a)**, for the relatively dense ground condition with a porosity of n = 0.3, the theoretical and numerical results are generally in good agreement. This consistency can be attributed to the fact that, as illustrated in **Fig. 7**, the grout penetration behavior at n = 0.3 remains in a permeation (bell-shaped) pattern across all injection pressures, without any transition to diffusion or fracturing. In contrast, for the loosest ground condition with n = 0.4, shown in **Fig. 10(c)**, noticeable discrepancies arise between the theoretical and numerical values at certain injection pressures. Specifically, from 550 kPa onward, the numerical results begin to fall below the theoretical predictions. This difference corresponds to the shift in grout behavior observed in **Fig. 7**, where penetration at 550 kPa still follows a bell-shaped permeation pattern, but transitions to a pot-shaped diffusion pattern at pressures of 600 kPa and above. This change signifies the onset of fracture grouting behavior beginning around 550 kPa. In conclusion, under dense ground conditions such as n = 0.3 where fracture grouting does not occur, the theoretical and numerical results show good agreement. However, in looser soils like n = 0.4, where fracture-based diffusion begins to develop, discrepancies between the theoretical model (which assumes permeation-only behavior) and the numerical simulation results become evident. Since the theoretical equation is based solely on permeation grouting, any occurrence of fracture grouting will naturally result in deviations from the theoretical prediction. **Fig. 10(b)** shows the results for n = 0.35, which exhibit an intermediate trend between those of n = 0.3 and n = 0.4. This suggests that partial fracture grouting may also occur under this condition.

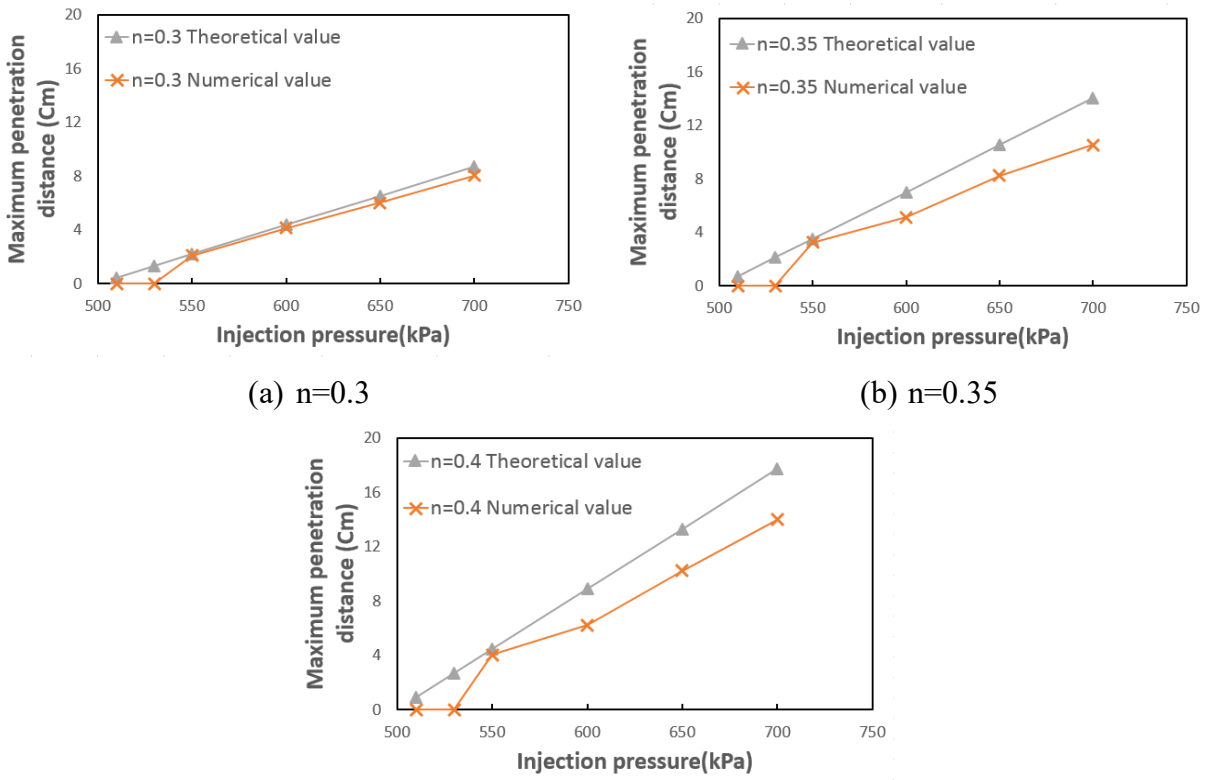

(a) n=0.3 (b) n=0.35

(c) n=0.4

Fig. 10 Comparison of Numerical and Theoretical Results

5. CONCLUSIONS

In this study, a numerical model was developed to simulate the injection of cement grout into the ground in front of a TBM face. In addition, a practical theoretical equation for estimating grout penetration distance was proposed based on a review of existing literature. Both the numerical analysis and the proposed theoretical model were applied to investigate the effects of varying grout injection pressures and ground conditions on the grout penetration distance and the water inflow quantity entering the TBM face. The final objective was to identify the boundary between permeation grouting and fracture (diffusion) grouting. The major findings of this study are summarized as follows

(1) In dense sandy soils, the water inflow reduction due to cement grout injection tended to increase gradually with higher injection pressures. In contrast, in loose sandy soils, the water inflow rate decreased significantly beyond a certain injection pressure. This indicates that, in dense soils, only permeation grouting occurred, resulting in a gradual reduction of inflow, whereas in loose soils, the grouting behavior shifted from permeation to fracture grouting at a certain pressure, leading to a sharp decrease in inflow.

(2) The grout penetration behavior under varying injection pressures and ground conditions was examined numerically. In dense ground, only bell-shaped permeation behavior was observed, whereas in loose soils, fracture-type (diffusive) grouting began to occur beyond a threshold injection pressure.

(3) A theoretical equation for estimation of the maximum grout penetration distance and permeability coefficient based on the Bingham fluid model, was formulated. Using this, the maximum penetration distance under various injection pressures and ground conditions was calculated, and the validity of the theoretical model was confirmed.

(4) A comparison between the grout penetration distances calculated using the theoretical model and those obtained from numerical analysis revealed good agreement under permeation-dominant conditions. However, discrepancies arose under ground conditions and pressures where fracture grouting occurred, as the theoretical model assumes only permeation grouting. This confirms the validity of both the proposed theoretical approach and the numerical simulation model.

(5) This study was conducted under the assumption of a 500 kPa overburden pressure in sandy ground. Therefore, the numerical values and outcomes may vary depending on specific ground and field conditions.

Acknowledgments

This work was supported by the National Research Foundation of Korea (NRF) grant funded by the Korea government (MSIT). (RS-2023-00208668206820732500001)

REFERENCES

ANSYS (2009), ANSYS FLUENT 12.0 User’s Guide, ANSYS FLUENT 12.0/12.1 Documentation

Benyounes, K. (2019), Rheological Behavior of Cement-Based Grout with Algerian Bentonite, SN Applied Sciences (1:1037).

Cubrinovski, Misko, and Ishihara, K. (1999), Empirical Correlation between SPT N-Value and Relative Density for Sandy Soils, Soils and Foundations (39:5), pp. 61–71.

Cubrinovski, Misko, and Ishihara, K. (2002), Maximum and Minimum Void Ratio Characteristics of Sands, Soils and Foundations (42:6), pp. 65–78.

Hwang, P.B., Kim, B.J. and Lee, S.W. (2024), TBM mechanical characteristics for NFGM in mechanized tunnelling, Geomechanics and Engineering, (38:5), pp.477-486.

Li, H., Ji, X. and Zhou, P. (2022), Study on the Microscopic Mechanism of Grouting in Saturated Water-Bearing Sand Stratum Based on VOF-DEM Method, Processes (10:8), pp. 1447.

Lee, J.W., Jo, H.W., Choi H.Y., and Oh, T.M. (2021), Analysis of Viscosity and Bleeding Characteristics of Ground Grouting Materials According to Bentonite Content, Land and Housing Research (12:4), pp. 127–137.

Raffle, J. F. and Greenwood, D. A. (1961), The Relationship Between the Rheological Characteristics of Grouts and Their Capacity to Permeate Soils, International Conference on Soil Mechanics and Foundation Engineering, (2:5), pp. 789-793.

Shepherd, R.G. (1989), Correlations of Permeability and Grain Size, Groundwater (27:5), pp. 633–638.

Petros P. Xanthakos, Lee W. Abramson, and Donald A. Bruce. (1994), Ground Control and Improvement: Permeation Grouting, Hoboken, NJ: John Wiley & Sons.